RSC Advances

ROYAL SOCIETY OF CHEMISTRY

www.rsc.org/advances

Amorphous Cu_2O/SnO_x/CNFs Composite Webs as Anode materials with Superior Lithium-ion storage Capability

Cheng Chi[1], Jinle Lan[1,2], Jiangman Sun[1], Yuan Liu[1], Yunhua Yu[1,2,*]and Xiaoping Yang[1,2]

[1] *State Key Laboratory of Organic-Inorganic Composites, Beijing University of Chemical Technology, Beijing 100029, China*

[2] *Changzhou Institute of Advanced Materials, Beijing University of Chemical Technology, Beijing 100029, China*

* Corresponding author. Tel. /Fax: +8610-6442-7698/2084

E-mail address: yuyh@mail.buct.edu.cn

GRAPHICAL ABSTRACT

Amorphous Cu_2O/SnO_x/CNFs Composite Webs as Anode materials with Superior Lithium-ion storage Capability

Cheng Chi[1], Jinle Lan[1,2], Jiangman Sun[1], Yuan Liu[1], Yunhua Yu[1,2,]*and Xiaoping Yang[1,2]

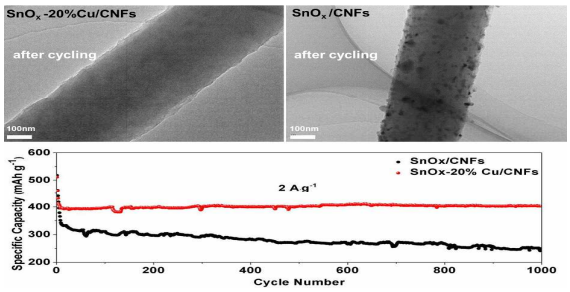

Cu-adding has a significant effect on restricting the aggregation of Sn particles during continuous charge/discharge progress and improve the cycling stability of the SnO_x/CNFs electrode.

Abstract

Amorphous Cuprous oxide/tin oxides/carbon nanofibers (Cu_2O/SnOx/CNFs) composite webs are prepared by electrospinning technique and subsequent thermal treatment. Cu-doped SnOx particles are uniformly distributed in the CNFs and maintain the original morphology after long-term cycling. In a controlled experiment, SnOx-20%Cu/CNFs with the atomic ratio of Cu:Sn = 0.2 shows the highest electrochemical performance with a high reversible capacity of 743 mA h g^{-1} at a current density of 200 mA g^{-1} and an excellent rate capacity of 347 mAh g^{-1} at 5 A g^{-1}. Moreover, the composite electrode exhibits an outstanding long-term cycling performance at 2 A g^{-1} even after 1000 cycles. The superior reversible lithium-ion storage capability is attributed to the unique structure of SnO_x dispersed in CNFs as well as the Cu-adding effects such as promoting electron transport and Li^+ diffusion, preventing Sn from aggregation during cycling, and improving the reversibility of Sn back to SnO_x in the recharge process.

Key words: Cuprous oxide, Tin oxides, Carbon nanofibers, electrospining, lithium-ion storage anodes

1. Introduction

Currently, tin oxides have attracted considerable attention as potential substitutes for commercial graphite anode materials in the development of high-performance lithium ion batteries (LIBs) because of their numerous appealing features, including low cost, abundance, environmental benignity, and high theoretical capacity (SnO: 880 mAh g^{-1}, SnO_2: 780 mAh g^{-1}).[1-6] However, the major drawback of quick capacity fading upon extended cycling renders them still unsuitable for replacement of the commercial graphite-based anode materials. This problem is believed to be associated with their poor electronic conductivity, large volume expansion, and severe aggregation during the charge-discharge processes, which result in a large irreversible capacity loss and poor rate performance, making it the biggest challenge for employing tin oxides as superior active anode materials in high energy and high power LIBs.

Many strategies have been adopted to improve the electrochemical performance of tin oxides. One of the useful strategies is to incorporate tin oxides with various carbonaceous materials, such as carbon nanofibers,[7] carbon nanotubes[8, 9] and graphene,[10-13] which not only accommodates the internal strain as an effective buffer layer, but also provides conductive paths to fasten the transfer of electrons. In particular, ultrafine SnO_x embedded carbon nanofibers (SnO_x/CNFs) show exceptional electrochemical property due to their unique one-dimentional (1D) nanostructure beneficial for electron and ion transport.[14] Nevertheless, the SnO_x/CNFs anode still yields unsatisfying high capacity and high-rate performance due to its initial large irreversible capacity and insufficient electronic conductivity. Based on this point, we have introduced titanium (Ti) and phosphorus (P) to SnO_x/CNFs and achieved Ti-doped SnO_x/CNFs and P-doped SnO_x/CNFs anode materials with enhanced capacity and high-rate performance.[15, 16] As reported in our studies and other previous

works on SnO_x/CNFs materials, the optimal carbonization temperature is usually limited to no more than 700℃, otherwise, higher carbonization temperature will generate the agglomeration of Sn particles, resulting in the pulverization of the electrode. However, the low electronic conductivity of amorphous CNFs carbonized up to 700℃ is insufficient to obtain high-rate performance. Therefore, it is highly desirable to develop an effective way to improve the rate performance of SnO_x/CNFs anode material without any agglomeration of Sn particles during carbonization. Various metallic heteroatoms adding has been envisaged and verified as an effective method to improve its low electronic properties, limited capacity and poor cycling stability.[17,18] Copper (Cu), with the second highest electrical conductivity after silver while being much cheaper, exposes itself as one of the most advisable candidates for heteroatom adding to achieve high rate capacity and excellent cycling performance of electrodes.[19, 20] It has been reported that the sandwich-stacked SnO_2/Cu hybrid nanosheets exhibit a high reversible capacity, stable cycling performance and superior rate capability, benefiting from high electron transport and fast ion diffusion. [21]

In this study, amorphous Cu_2O/SnO_x/CNFs composite webs with different amounts of Cu-adding were prepared by electrospinning technique and subsequent thermal treatment. An optimal Cu-added SnO_x/CNFs anode (SnO_x-20%Cu/CNFs) with a high reversible capacity (743 mA h g^{-1} at a current density of 200 mA g^{-1}) and a superior rate capability (347 mAh g^{-1} at 5 A g^{-1}) was obtained. The effects of Cu-adding on the electrochemical performance of the as-prepared Cu_2O/SnO_x/CNFs webs were investigated, and the underlying mechanism were explained in detail.

2. Experimental

2.1 Preparation of Cu_2O/SnO_x/CNFs composite webs

Typically, 2.0 g polyacrylonitrile (PAN, Petro China Jilin Petrochemical Co.) was dissolved into

20 ml N, N-dimethylformamide (DMF, Beijing Chemical Co.) at 50 °C for 24 h (Solution A). Then 0.44g copper dichloride ($CuCl_2 \cdot 2H_2O$, Beijing Chemical Co.) and 1.5 ml anhydrous tin tetrachloride ($SnCl_4$, Beijing Chemical Co.) were mixed with a Cu/Sn molar ratio of 0.2 into 4.8 ml ethylene glycol (EG, Beijing Chemical Co.) (Solution B). After that, solution A was added in solution B under continuously magnetic stirring for 24 h to obtain precursor solution for eletrospinning. Electrospinning was carried out with an electrostatic voltage of 15 kV, a feeding rate of 0.3 ml h^{-1}, and a collecting distance of 15cm. The as-prepared nanofiber webs were stabilized at 270 °C for 3 h in air, and then carbonized at 700 °C for 1 h under a high-purity nitrogen atmosphere to obtain the Cu_2O/SnO_x/CNFs composite webs, which is denoted as SnO_x-20%Cu/CNFs based on the Cu/Sn molar ratio of 0.2. Similarly, other two Cu-added SnO_x/CNFs samples with a varied Cu/Sn molar ratio (Cu/Sn=0.1 and 0.3) and pristine SnO_x/CNFs were prepared under the same conditions, correspondingly denoted as SnO_x-10%Cu/CNFs, SnO_x-30%Cu/CNFs and SnO_x/CNFs, respectively.

2.2. Characterizations of Cu-doped SnOx/CNFs composite webs

Morphologies and elemental composition of the as-prepared samples were observed and evaluated using a field emission scanning electron microscope (FE-SEM, Supra55, Carl Zeiss) with energy dispersive X-ray (EDX) spectroscopy. A single nanofiber was observed with a high resolution transmission electron microscope (HR-TEM, JEM-3010, JEOL), and HR-TEM mapping was conducted on the same filament to observe the distribution of elements. Thermogravimetric analysis (TGA) was carried out on a TGA instrument (TA-Q50, America) at a heating rate of 10 °C min^{-1} from room temperature to 800 °C under air atmosphere to determine the contents of components in sample. The crystal structures of samples were investigated by X-ray diffraction (D8 Advance, Brucker, Cu Kα, λ=0.154 nm). Raman spectroscopy was recorded on a Renishaw inVia with 514 nm

diode laser excitation. X-ray photoelectron spectroscope (XPS, EscaLab 250, Thermo Fisher Scientific) and AES (Auger electron spectroscope) using monochromatic Al Kα (1486.6 eV) X-ray as the excitation source were employed to analyze the elemental chemical status of the samples.

2.3. Electrochemical performance measurements

Electrochemical performance measurements were carried out using CR2025 coin cells with lithium as counter and reference electrode, Celgard 2300 membrane as separator, and 1 M $LiPF_6$ in ethylene carbonate (EC)/dimethyl carbonate (DMC) (1:1 v/v) as electrolyte under ambient temperature. All of cells were assembled in an argon-filled glove box (OMNI-LAB). The electrochemical performances of the half coin cells were evaluated on a battery tester (LAND CT2001A) at a constant current density of 200 mA g^{-1} and variable current densities of 100, 200, 500, 1000, 2000 and 5000 mA g^{-1} over the potential range from 0.005 to 3.0 V. Cyclic voltammetry (CV) measurements were performed between 0.005 and 3.0 V using an electrochemical workstation (Autolab PGSTAT 302 N, Metrohm) at different scan rate of 0.1, 0.5, 1, 3, and 5 mV s^{-1}. Electrochemical impedance spectroscopy (EIS) was investigated on the same workstation over the frequency range of 100 kHz to 0.01 Hz.

3. Results and discussion

Figure 1 shows the morphology and elemental composition of SnO_x-20%Cu/CNFs webs. The SEM image in Figure 1a displays continuous and uniform fibrous morphology of SnO_x-20%Cu/CNFs with a diameter range of 200–300 nm. The sample presents smooth surface without agglomerated nanoparticles, indicating that the Cu-added SnO_x particles are well embedded in CNFs matrix. The contents of Cu-added SnO_x particles in SnO_x-20%Cu/CNFs is determined to be about 22.7 wt% by TGA measurements (Figure S1，Supporting Information). The content of

Cu-adding has no significant effect on the morphologies of SnO_x/CNFs, as shown in Figure S2 (Supporting Information). HR-TEM was used to further detect the existence of Cu-added SnO_x particles. As shown in Figure 1b and 1c, it is difficult to identify any particle on CNFs even at high resolution (Figure 1c), which certifies the existence of ultrafine Cu-added SnO_x particles in CNFs matrix. Furthermore, no clear diffraction rings or dots were detected from the selected area electron diffraction (SAED) pattern of the SnO_x-20%Cu/CNFs (inset of Figure 1b), indicative of an amorphous state of Cu-added SnO_x. Based on the semi-quantitative estimation of EDX as shown in Figure 1d, the molar ratio of Cu/Sn is calculated to 0.22, which is similar to the nominal molar ratio of 0.2, and the contents of Sn and Cu in SnO_x-20%Cu/CNFs are 17.82 wt% and 2.15 wt%. To further investigate the distribution of Cu-added SnO_x particles in CNFs, elemental mappings of carbon, oxygen, tin and copper were performed on the SnO_x-20%Cu/CNFs. As shown in Figure 1f-I, Sn, Cu and O elements distribute homogeneously along the CNFs, which is beneficial for the electrochemical performance of Cu-added SnO_x /CNFs electrodes.[22]

Figure 2a shows the X-ray diffraction (XRD) patterns of the Cu-added SnO_x/CNFs with different Cu-adding contents. All of the samples exhibit a broad peak near 25°, corresponding to the amorphous graphitic carbon. Moreover, no any clear peaks assigning to SnO_x are detected in the samples, showing the amorphous nature of SnO_x particles, which is coincided with the result of the inset in Figure 1b. The Raman spectra of all samples in Figure 2b show two distinct peaks near 1357 cm^{-1} and 1580 cm^{-1}, which correspond to D-band and G-band of carbonaceous materials. The ratio of D and G intensity (I_D/I_G) of all samples is calculated to be about 1.1, indicating the high disordered and low graphitization degree of CNFs，which is favorable for enhancing lithium storage and transfer by providing more electro-active sites in bulk electrodes.[23]

X-ray photoelectron spectroscopy (XPS) was used to investigate the electronic state and the composition of Cu-added SnO_x/CNFs samples. As shown in Figure 3a, the XPS spectra of both SnO_x/CNFs and SnO_x-20%Cu/CNFs present the signals of C, N, O and Sn elements, and Cu 2p peak was detected in SnO_x-20%Cu/CNFs.[24, 25] In the high-resolution XPS spectra of Sn 3d for SnO_x/CNFs and SnO_x-20%Cu/CNFs (Figure 3b), the Sn $3d_{5/2}$ was decomposed to three peaks with binding energy (BE) of 487.5 eV, 486.7 eV, and 484.7eV, which are assigned to the Sn^{4+}, Sn^{2+} and Sn^0, respectively.[26] The proportions of Sn^0, Sn^{2+} and Sn^{4+} for SnO_x-20%Cu/CNFs are 11.14%, 71.83% and 17.03%, respectively, which are similar to those of SnO_x/CNFs sample (9.67%, 69.95%, and 20.38%), demonstrating that Cu-adding has no significant effect on the valence state of Sn. In the high-resolution XPS spectra of Cu $2p_{3/2}$ for the SnO_x-20%Cu/CNFs sample, as shown in Figure 2c, a high intensity of the peak at ~ 932.3 eV is corresponding to Cu^+ or metallic Cu.[27] The Auger Cu LMM spectrum can be used to distinguish between Cu^+ and metallic Cu. In Figure 3d, a high intensity of the peak at ~ 916.5 eV is observed from the Auger Cu LMM spectrum. Auger parameter refers to the sum of the binding energy of the strongest photoelectron peak from XPS and the kinetic energy of the sharpest Auger peak from AES. In Figure 3d, the measured Auger parameter (932.3eV+916.5eV=1848.8 eV) of Cu in SnO_x-20%Cu/CNFs, which is closer to the reference value of the Auger parameter of Cu_2O (1849 eV) rather than that of metallic Cu (1851 eV), indicates that the added copper exists in the form of Cu^+.[28]

Figure 4a and 4b show CV curves for the initial three cycles of SnO_x/CNFs and SnO_x-20%Cu/CNFs electrodes under the voltage ranging from 0.005 to 3.0 V vs Li^+/Li with a scan rate of 0.1 mv S^{-1}. The electrochemical reactions of SnO_x are described by the following equations.[29]

$$SnO_x + 2xLi^+ + 2xe^- \rightarrow Sn + xLi_2O \ (x \leq 2) \qquad (1)$$

$$Sn + xLi^+ + xe^- \leftrightarrow Li_xSn \ (x \leq 4.4) \quad (2)$$

In Figure 4a and 4b, the cathodic peaks observed in the first cycle at 0.6 V and 0.2V correspond to the formation of SEI film as well as the reduction of SnO_x to Sn and the intercalation of Li^+ into the CNFs. Peaks at 0.45 V and 0.55 V (Peak 1) in the first discharge and charge process are attributed to the reversible alloying and de-alloying reaction of Sn in the reaction (2). An anodic peak locating around 1.2 V (Peak 2) in the first charge process is assigned to the electrochemical inverse process of reaction (1), a critical step on the reversibility of SnO_x. It was found that SnO_x-20%Cu/CNFs presented a higher current intensity of Peak 2 than that of SnO_x/CNFs, indicating the improved reversible capability of the conversion reaction (1) for SnO_x-20%Cu/CNFs, which contributes to the first coulombic efficiency and reversible capacity of the electrodes. Figure 4c shows a series of voltammetric curves of SnO_x-20%Cu/CNFs and SnO_x/CNFs recorded as a function of v in the range from 0.5 to 5 mV s^{-1}. As shown in Figure 4c, the current density of Peak 2 of SnO_x-20%Cu/CNFs is always larger than that of SnO_x/CNFs with the increase of scan rates, indicating a good reversibility of the conversion reaction (1) for SnO_x-20%Cu/CNFs. Moreover, the electrode potentials of SnO_x-20%Cu/CNFs at the peak 1 and Peak 2 are always lower than those of SnO_x/CNFs, suggesting that SnO_x-20%Cu/CNFs possesses a low electrode polarization and a higher Li^+ diffusivity than SnO_x/CNFs. Figure 4d shows the peak current (Ip, the peak near 1.2 V) plotted as a function of the root of the scan rate ($v^{1/2}$). It can be seen that the peak currents of both SnO_x/CNFs and SnO_x-20%Cu/CNFs electrodes are approximately proportional to the root of the scan rate ($v^{1/2}$). According to the Randles-Sevcik equation, $Ip = (2.69\times10^5)n^{3/2}D^{1/2}C_0v^{1/2}$, where n is the number of electrons per molecule during the intercalation, C_0 is the concentration of lithium ions, D is the diffusion coefficient, and v is the scan rate, the reaction kinetics are controlled by the Li^+ diffusion

step.[30] As shown in Fig 4d , SnO_x-20%Cu/CNFs electrode shows a higher slope than that of SnO_x/CNFs, indicating a larger Li^+ diffusion coefficient (D), which is beneficial for the rate performance of electrodes.

Figure 5a and 5b show the galvanostatic charge-discharge profiles of SnO_x/CNFs and SnO_x-20%Cu/CNFs. As shown in Figure 5a, the pristine SnO_x/CNFs present the first discharge and charge capacities of 1129 mAh g^{-1} and 841 mAh g^{-1}, corresponding to a coulombic efficiency of 74.5%. In Figure 5b, the SnO_x-20%Cu/CNFs show the first discharge and charge capacities of 1110 and 904 mAh g^{-1}, corresponding to a higher coulombic efficiency of 81.4% , which is increased by 6.9% compared with that of SnO_x/CNFs. The initial irreversible capacity loss mainly originates from the formation of solid electrolyte interphase (SEI) film on the surface of electrodes and the partial irreversible conversion reaction of SnO_x to Sn and inactive Li_2O.[31] The increase in the initial coulombic efficiency and reversible capacity for SnO_x-20%Cu/CNFs is attributed to the reversible electrochemical reaction of Cu_2O ($Cu_2O + 2Li^+ \leftrightarrow 2Cu + Li_2O$),[32] which producing metallic Cu during cycling, and make extra Li_2O reversibly convert to Li^+, giving the electrodes higher coulombic efficiency and reversible capacity in the first cycle. The fact that Cu_2O is reduced to metallic Cu in the first discharge cycle is confirmed by the XPS and AES spectra of SnO_x-20%Cu/CNFs at 0V in the first discharge progress (Figure S3 Supporting Information).[27] Figure 5c shows the cycling performance of the Cu-added SnO_x/CNFs and SnO_x/CNFs electrodes at 200 mA g^{-1} current density. In comparison with the SnO_x/CNFs electrode, the Cu-added SnO_x/CNFs electrodes exhibit a varying degree of enhancement in cycling capacity with Cu-doping content. The SnO_x-20%Cu/CNFs electrode exhibits the highest reversible capacity of 743 mA h g^{-1} after the 100th cycle compared with the capacities of 652 mA h g^{-1}, 719 mA h g^{-1}, and 665 mA h g^{-1} for SnO_x/CNFs,

SnO_x-10%Cu/CNFs, and SnO_x-30%Cu/CNFs, respectively. Obviously, once the Cu-doping content exceeds to a certain value, the reversible capacity of the Cu-doped SnO_x/CNFs electrode becomes lower due to the existence of more Cu_2O, which has a lower theoretical specific capacity (375 mA h g-1) than that of SnO_x (Sn: 992 mA h g^{-1}; SnO: 875 mA h g^{-1}; SnO_2: 782 mA h g^{-1}). In this work, the optimal SnO_x-20%Cu/CNFs electrode with a Cu/Sn molar ratio of 0.2 was obtained. Figure 5d shows the rate performance of all electrodes at different current densities. It can be seen that the SnO_x-20%Cu/CNFs electrode also presents the highest rate capacities at different current densities among all the samples. Especially, at the high current density of 5 A g^{-1}, the SnO_x-20%Cu/CNFs electrode retains a specific capacity as high as 347 mAh g^{-1}, which is 62.1% higher than that of SnO_x/CNFs electrode (214 mAh g^{-1}). Moreover, the SnO_x-20%Cu/CNFs electrode exhibits an excellent cycling stability at high charge/discharge rate. As shown in Figure 5d, after 1000 cycles at 2 A g^{-1}, the SnO_x-20%Cu/CNFs electrode still delivers a high reversible capacity of 411 mAh g^{-1}. The excellent long-term cycling and high-rate performance of the SnO_x-20%Cu/CNFs electrode are ascribed to the in situ formation of metallic Cu during cycling, which increases the electrical conductivity of the electrode because of the high electrical conductivity of Cu (6×10^{7} S m^{-1}) at room temperature.

To further probe the enhanced rate capability, electrochemical impedance spectroscopy (EIS) measurements were carried out after three cycles, and the obtained Nyquist plots are shown in Figure 6. The intercept at the Zreal axis at high frequency corresponds to the ohmic resistance (R_Ω), which represents the total resistance of the electrolyte, separator, and electrical contacts. The semicircle in the middle frequency range indicates the charge transfer resistance (Rct), and the inclined line in the low-frequency range represents the Warburg impedance. The semicircle for SnO_x-20%Cu/CNFs

electrode is much smaller than that of SnO_x/CNFs electrode. R_{ct} value (191.3Ω) of the SnOx-20%Cu/CNFs is much smaller than that of the SnO_x/CNFs (389.6Ω), corresponding to the exchange current densities i_0 calculated based on the following equation [12]:

$$i_0=RT/nFR_{ct}A \qquad (3)$$

Obviously, compared with the SnOx-20%Cu/CNFs electrode, the SnOx-20%Cu/CNFs electrode gives the easier and faster charge, indicating that the incorporation of Cu^+ into SnO_x can greatly improve the charge transfer ability of Li^+ at the interface between the electrolyte and electrode and the conductivity of the electrode, leading to the superior rate capability of SnO_x-20%Cu/CNFs electrode. The metallic tin and copper produced by the reduction of SnO_x-Cu_2O with Li^+ can maintain higher electrical conductivity than the single metallic tin of SnO_x/CNFs composite. Since the faradic reaction is determined by ion transfer and electron conduction, the reduction of the resistance can be attributed to the improved electronic conductivity of the composite electrodes induced by the metallic Cu. The electrochemical polarization of the Cu_2O/SnOx/CNFs electrode was greatly reduced compared with the pure SnO_x/CNFs electrode. Moreover, carbon nanofibers in the presence of Cu_2O/SnOx/CNFs acts as a conductive buffer-spacer which improves the electron transport property of the electrode and stabilizes the electronic and ionic conductivity, therefore leading to fast lithium ion diffusion and low charge transfer resistance. This result is also in agreement with the superior rate capability of Cu_2O/SnO_x/CNFs since charge transfer process is the rate-determining step for conversion reactions [27].

To further understand the outstanding electrochemical performance of the as-prepared SnO_x-20%Cu/CNFs electrode, HR-TEM analysis was conducted to observe the morphological change of SnO_x-20%Cu/CNFs and SnO_x/CNFs electrodes after 1000 charge/discharge cycles at 2A

g^{-1}. It is clearly seen from Figure 7 that both SnO_x/CNFs and SnO_x-20%Cu/CNFs electrodes maintain the original fibrous morphology with no obvious pulverization or cracking after 1000 cycles, however, their internal structures exhibit significant difference. Figure 7a-c show that SnO_x and Cu_2O are still well-dispersed in CNFs and remains perfect amorphous structure without any aggregation even after 1000 cycles for SnO_x-20%Cu/CNFs, while large numbers of nanoparticles are aggregated on the surface of CNFs in SnO_x/CNFs due to the aggregation of Sn particles during long-term cycling, as shown in Figure 7d-f, indicating that Cu-doping also plays a significant role in restricting the aggregation of Sn particles in SnO_x-20%Cu/CNFs during charge/discharge cycling.

The remarkable electrochemical performance, especially the high cycling capacity and excellent rate performance of the as-prepared Cu_2O/SnO_x/CNFs electrodes, should be associated with the following facts. Firstly, the incorporation of Cu^+ into SnO_x/CNFs can greatly improve the charge transfer ability of Li^+ at the interface between the electrolyte and electrode and the conductivity of the electrode. Secondly, the reduction of Cu_2O through the discharge progress leads to the formation of Cu nanoparticles dispersed in a lithiamatrix (Li_2O), inhibiting the aggregation of Sn particles in the following alloying–dealloying cycling. Meanwhile, the presence of Cu nanoparticles with high surface activity can enhance the reactivity of Li_2O decomposition, and improve the reversibility of Sn back to SnO_x in the recharge process.

4. Conclusion

Cu_2O/SnO_x/CNFs composite anode materials with superior lithium-ion storage capability have been synthesized via a facile electrospinning method and subsequent thermal treatment. The as-prepared Cu_2O/SnO_x/CNFs composite is characterized by a structure with the uniform dispersion of ultrafine

amorphous Cu_2O/SnO_x/CNFs nanoparticles in CNFs matrix. On one hand, the ultrafine and uniformly dispersed Cu_2O/SnO_x/CNFs nanoparticles can provide large numbers of active sites for lithium storage and shorten the diffusion length of lithium ions. On the other hand, the incorporation of Cu^+ into SnO_x/CNFs can lead to the formation of Cu nanoparticles dispersed in a lithiamatrix (Li_2O), inhibiting the aggregation of Sn particles in the following alloying–dealloying cycling. Meanwhile, the presence of Cu nanoparticles can not only improve the charge transfer ability of Li^+ and the conductivity of the electrode, but also enhance the reversibility of Sn back to SnO_x in the recharge process, Therefore, Cu-adding can greatly enhance the reversible capacity and rate capability of the SnO_x/CNFs electrode, and an optimal Cu_2O/SnO_x/CNFs composite anode material with the atomic ratio of Cu: Sn = 0.2 (SnO_x-20%Cu/CNFs) has been obtained. The optimum electrode exhibits a greatly enhanced reversible capacity (743 mA h g^{-1} after 100 cycles at 200mA g^{-1}) and rate capability (347 mA h g^{-1} at 5A g^{-1}) compared with the pristine SnO_x/CNFs electrode, showing the potential as a high-performance anode materials for lithium-ion batteries.

Acknowledgments

This work was financially supported by National Natural Science Foundation of China (No. 51072013, 51272021 and 51102009) and Natural Science Foundation of Jiangsu Province (No. BK20131147).

Reference

(1) J.S. Chen, X.W. Lou, Small, 2013, **9**, 1877.

(2) L. Zou, L. Gan, R.T. Lv, M.X. Wang, Z.H. Huang, Z. F.Y. Kang, W.C. Shen, Carbon, 2011, **49**, 89.

(3).Z.H. Wen, S.M. Cui, H.J. Kim, S. Mao, K.H. Mao, G.H. Lu, H.H. Pu, O. Mao, J.H. Chen. J. Mater. Chem., 2012, **22**, 3300-3306.

(4) L.W. Ji, Z.K. T, T.Kuykendall, E.J. An, Y.B. Fu, V. Battaglia, Y.G. Zhang, Energy. Environ. Sci., 2011, **4**, 3611.

(5) X.S. Zhou, L.J. Wan, Y.G. Guo, Adv. Mater., 2013, **25**, 2152.

(6) D. Deng, J.Y. Lee. Chem. Mat., 2008, **20**, 1841.

(7) L. Zhang, G.Q. Zhang, H.B. Wu, L. Yu, X.W. Lou, Adv. Mater., 2013, **25**, 2589.

(8) H.Y. Mi, Y.L. Xu, W. Shi, H.D. Yoo, S.J. Park, Y.W. Park, S.M. Oh, J. Mater. Chem., 2011**, 21**, 19302.

(9) X. Li, T. Li, Q. Zhong, X.Zhang, H. Li, J. Huang. Mater. Lett., 2014, **130**, 232.

(10) H. Zhang, H. Song, X. Chen, J. Zhou, H. Zhang, Electrochim. Acta, 2012, **59**, 160.

(11) J.F. Liang, W. Wei, D. Zhong, Q.L. Yang, L.D. Li, L. Guo, ACS Appl. Mater. Interfaces, 2012, **4**, 454.

(12) C. Zhong, J.Z. Wang, Z.X. Chen, H.K. Liu, J. Phys. Chem. C, 2011, **115**, 25115.

(13) S.M, Paek, E.J. Yoo, I, Honma. Nano Lett., 2009, **9**, 72.

(14) B. Zhang, Y. Yu, Z.D. Huang, Energy Environ. Sci., 2012, **5**, 9895.

(15) Y. Liu, X. Yan, J.L. Lan, D. Teng, Y. Yu, X. Yang, Electrochim. Acta, 2014*,* **137**, 9.

(16) X. Liu, D. Teng, T. Li, Y. Yu, X. Shao, X. Yang, J. Power Sources, 2014, **272**, 614.

(17) H. Xia, C.Y. Hong, X.Q. Shi, B. Li, G.L. Yuan, Q.F. Yao, J.P. Xie. J. Mater. Chem. A, 2015, **3**, 1216.

(18) H. Xia, D.D. Zhu, Z.T. Luo, Y. Yu, X.Q. Shi, G.L. Yuan, J.P. Xie. Scientific Reports, 2013, **3**, 2978.

(19) H. El-Shinawi, M. Böhm, T. Leichtweiß, K. Peppler, J. Janek, Electrochem. Commun., 2013, **36**, 33.

(20) C. Li, W. Wei, S. Fang, H. Wang, Y. Zhang, Y. Gui, R. Chen, J. Power Sources, 2010, **195**, 2939.

(21) J.W. Deng, C.L. Yan, L.C. Yang, S. Baunack, S. Oswald, H. Wendrock, Y.F. Mei, O.G. Schmidt, ACS nano, 2013, **7**, 6948.

(22) J.S. Chen, Y.L. Tan, C.M. Li, Y.L. Cheah, D. Luan, S. Madhavi, X.W. Lou, J. Am. Chem. Soc.**,** 2010, **132**, 6124.

(23) L. Qie, W.M. Chen, Z.H. Wang, Q.G. Shao, X, Li, L.X. Hu, W.X. Zhang, Y.H. Huang. Adv. Mater., 2012, **24**, 2047.

(24) Y.G. Kang, H.J. Kim, H.G. Park, B.Y. Kim, D.S. Seo. J. Mater. Chem., 2012, **22**, 15969.

(25) K.K.H. Yu, K.S.M. Pillai, P.R. Nalla, O. Chyan, J. Appl. Electrochem., 2010, 40, 143.

(26) H. Liu, R.Z. Hu, W. Sun, M.Q. Zeng, J.W. Liu, L.C. Yang, M. Zhu. J. Power Sources, 2013, **242**, 114.

(27) D. Tahir, S. Tougaard, J. Phys.: Condens. Matter., 2012, **24**, 175001.

(28) H. El-Shinawi, M. Böhm, T. Leichtweiß, K. Peppler, J. Janek, Electrochem. Commun.**,** 2013, **36**, 33.

(29) J. Yao, X. Shen, B. Wang, H. Liu, G. Wang, Electrochem Commun., 2009, **11**, 1849.

(30) R. Hu, H. Liu, M. Zeng, J. Liu, M. Zhu, J. Mater. Chem., 2012, **22**, 9539.

(31) J. S. Chen, C.M. Li, W.W. Zhou, Q.Y. Yan, L. A. Archer, X.W. Lou, Nanoscale, 2009, **1**, 280.

(32) J.Y. Xiang, X.L. Wang, X.H. Xia, L. Zhang, Y. Zhou, S.J. Shi, J.P. Tu, Electrochim. Acta, 2010, **55**, 4921.

Figure captions:

Figure 1. Morphologies and elemental composition of SnO_x-20%Cu/CNFs: (a) SEM images; (b)(c) HRTEM images (with corresponding SAED patterns (inset)); (d) EDX analysis; and (e)-(i) elemental mapping of carbon, oxygen, tin, copper, respectively.

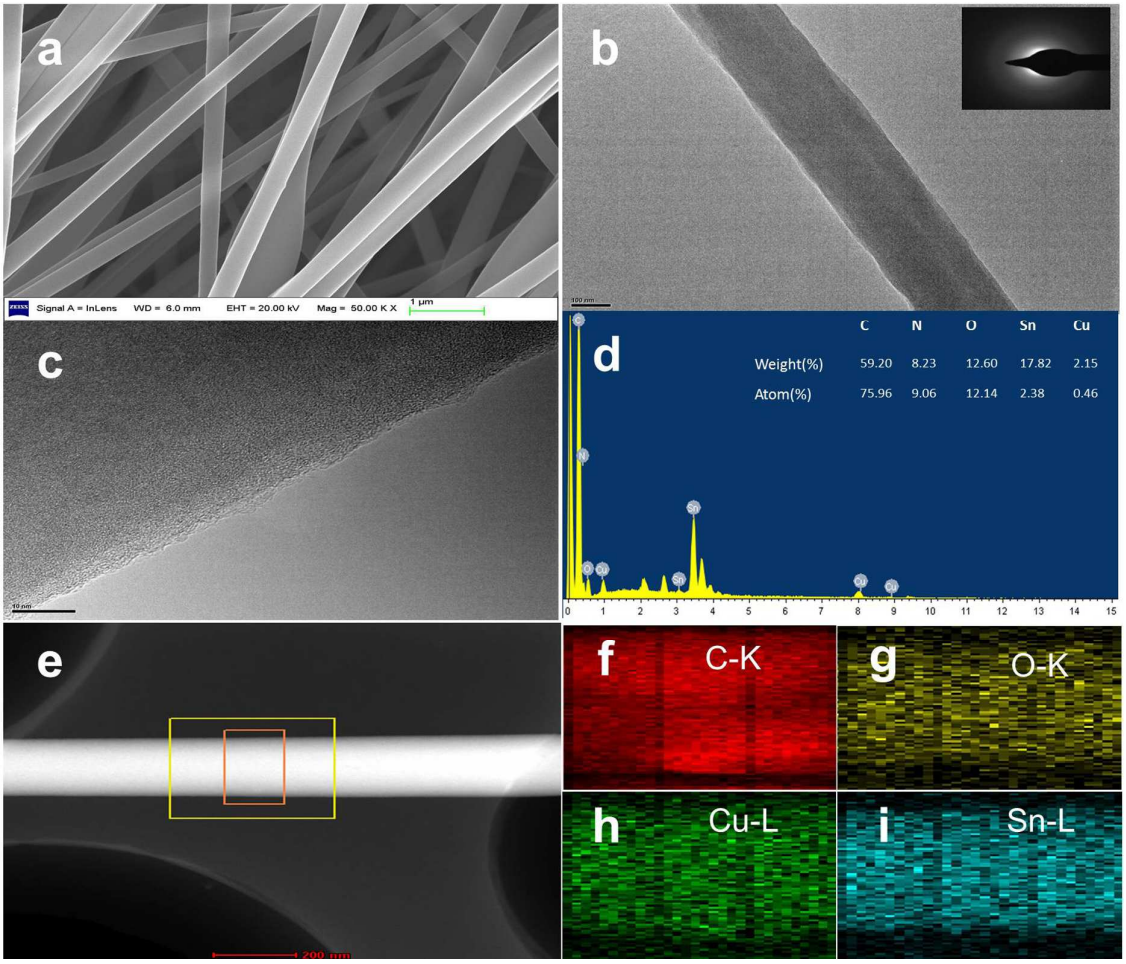

Figure 2. (a) X-ray diffraction (XRD) patterns of SnO_x/CNFs, SnO_x-10%Cu/CNFs, SnO_x-20%Cu/CNFs and SnO_x-30%Cu/CNFs; (b) Raman Spectroscopy of SnO_x/CNFs, SnO_x-10%Cu/CNFs, SnO_x-20%Cu/CNFs and SnO_x-30%Cu/CNFs.

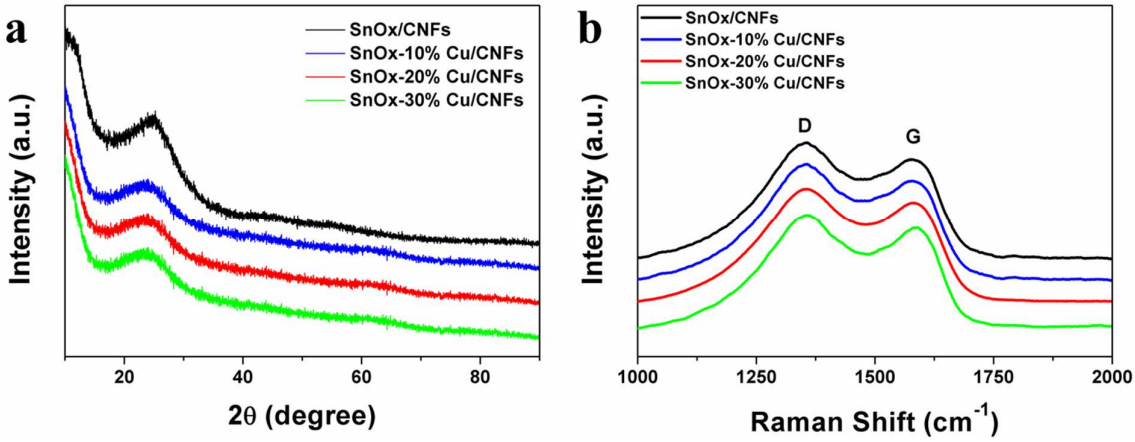

Figure 3. (a) XPS general spectra of SnO_x-20%Cu/CNFs and SnO_x/CNFs; (b) XPS high-resolution spectra of Sn 3d regions of SnOx-20%Cu/CNFs and SnO_x/CNFs and (c) XPS high-resolution spectra of Cu 2p regions of SnO_x-20%Cu/CNFs; (d) AES Spectra of Cu LMM Auger electron of SnO_x-20%Cu/CNF.

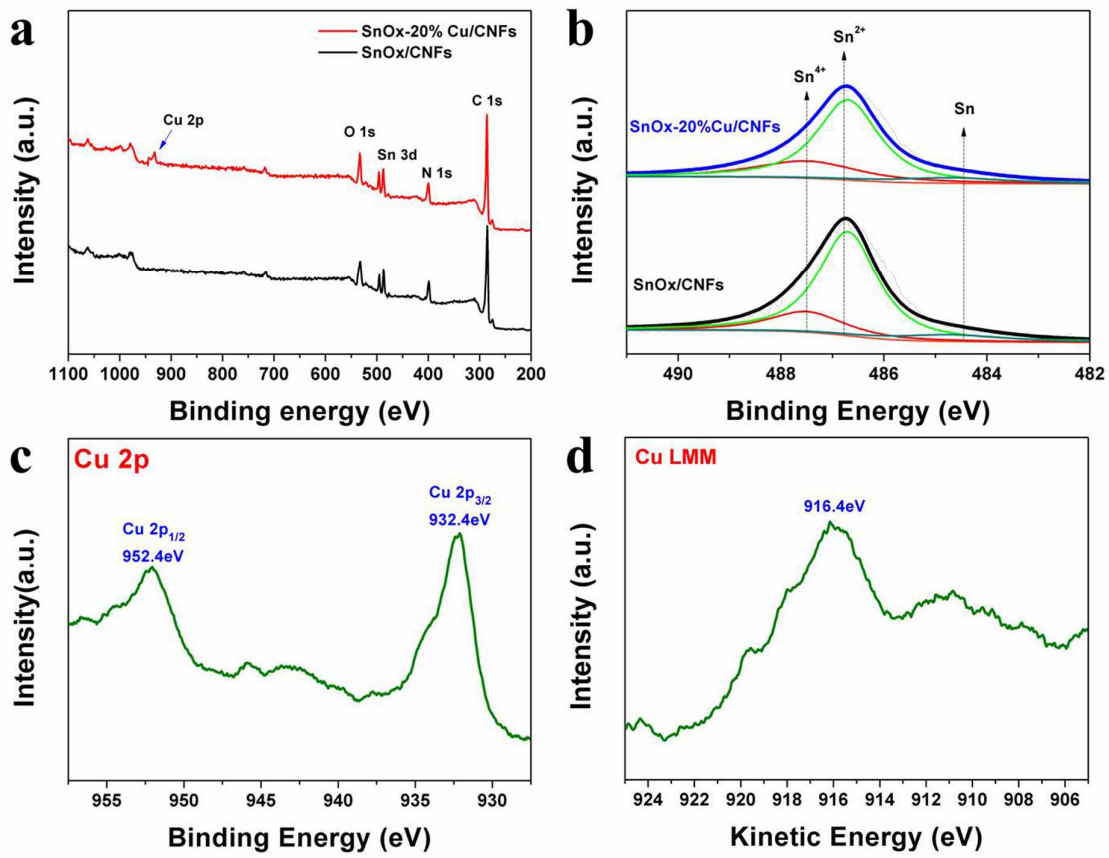

Figure 4. The initial three CV curves of (a) SnO_x/CNFs and (b) SnO_x-20%Cu/CNFs

scanned at 0.1 mV s^{-1}; (c) CV curves of SnO_x/CNFs and SnO_x-20%Cu/CNFs scanned at 0.5, 1, 3 and 5 mV s^{-1} after 5th, 10th, 15th, 20th, respectively; (d) I_p-$v^{1/2}$ curves of SnO_x/CNFs and SnO_x-20%Cu/CNFs.

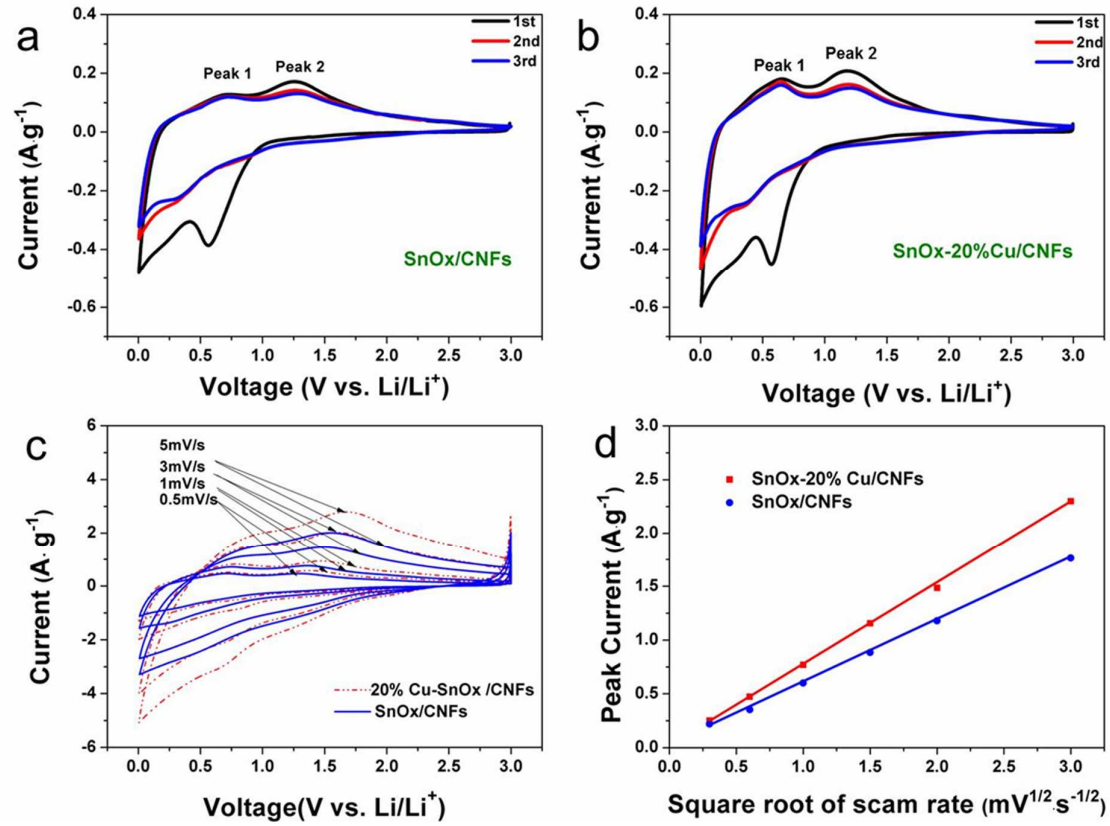

Figure 5. Charge-discharge curves of (a) SnO_x/CNFs and (b) SnO_x-20%Cu/CNFs cycled at 200 mA g^{-1}; (c) Cyclic performances of all samples at 200 mA g^{-1}; (d) Rate capability at different current rates of all samples; (e) long-term cycling performance of SnO_x/CNFs and SnO_x-20%Cu/CNFs.

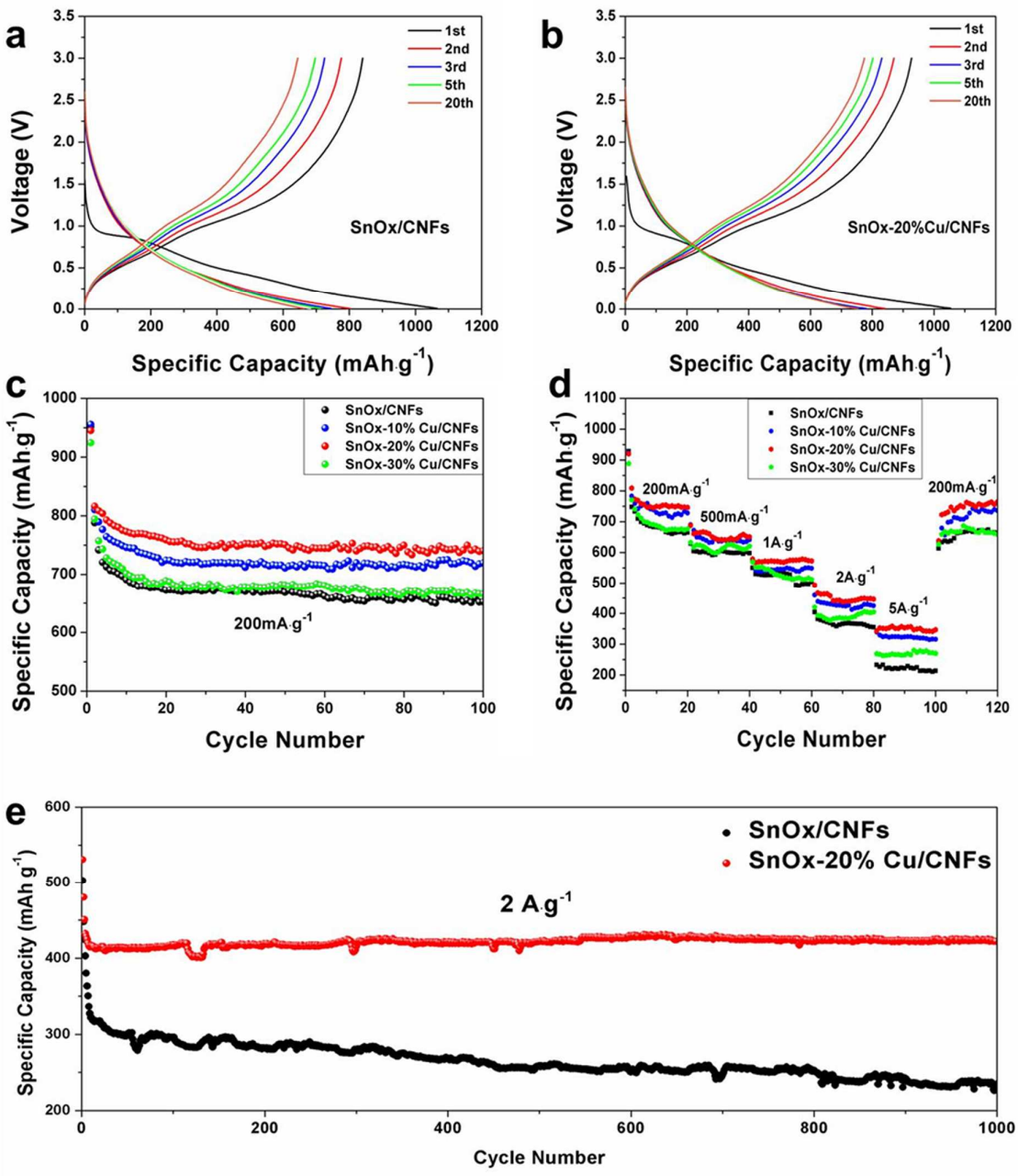

Figure 6. Nyquist plots performance of all samples in the full delithiated state after 3 cycles.

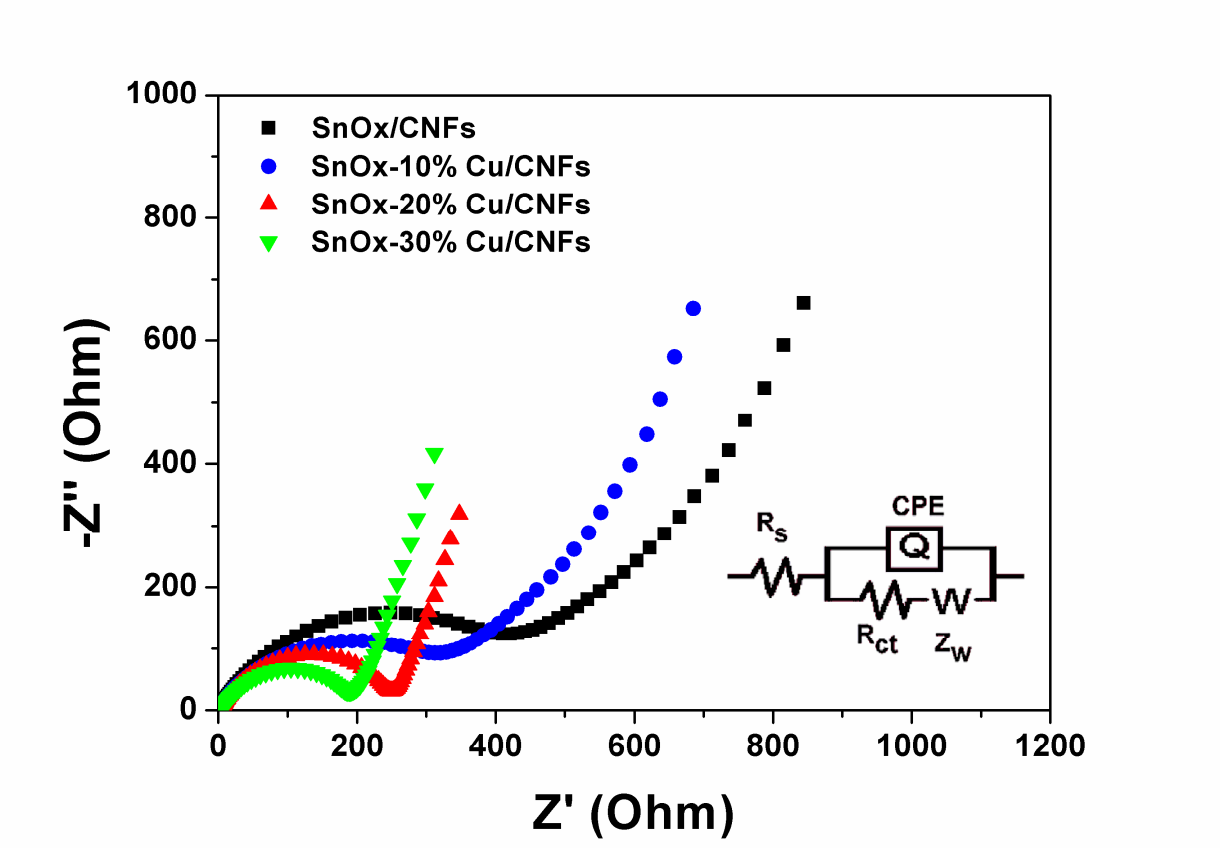

Figure 7. HRTEM images of (a)(b) SnO_x/CNFs and corresponding SAED pattern; HRTEM of (d)(e) SnO_x-20%Cu/CNFs and corresponding SAED pattern after 1000 cycle performance test at current density of 2A g^{-1}.